AGU PUBLICATIONS

Geophysical Research Letters

RESEARCH LETTER
10.1002/2015GL064347

**Key Points:**
- Northern and Southern Tibet deform similarly
- Tibetan crust thins rapidly
- Extrapolated to 10–15 Ma, Tibetan elevations dropped 1000 m

**Supporting Information:**
- Table S1

**Correspondence to:**
P. Molnar,
molnar@colorado.edu

**Citation:**
Ge, W.-P., P. Molnar, Z.-K. Shen, and Q. Li (2015), Present-day crustal thinning in the southern and northern Tibetan Plateau revealed by GPS measurements, *Geophys. Res. Lett.*, *42*, 5227–5235, doi:10.1002/2015GL064347.

Received 27 APR 2015
Accepted 5 JUN 2015
Accepted article online 8 JUN 2015
Published online 4 JUL 2015



# Present-day crustal thinning in the southern and northern Tibetan Plateau revealed by GPS measurements

**Wei-Peng Ge[1,2], Peter Molnar[3], Zheng-Kang Shen[4,5], and Qiang Li[6]**

[1]State Key Laboratory of Earthquake Dynamics, Institute of Geology, China Earthquake Administration, Beijing, China, [2]Lanzhou Institute of Seismology, China Earthquake Administration, Lanzhou, China, [3]Department of Geological Sciences and Cooperative Institute for Research in Environmental Sciences, University of Colorado Boulder, Boulder, Colorado, USA, [4]Department of Earth, Planetary, and Space Sciences, University of California, Los Angeles, California, USA, [5]Department of Geophysics, School of Earth and Space Sciences, Peking University, Beijing, China, [6]National Infrastructure of Earthquake Centre, China Earthquake Administration, Beijing, China

**Abstract** GPS measurements from sites within the Tibetan Plateau show not only east-southeast-west-northwest extension but also, more importantly, horizontal dilation throughout the interior of the plateau. Assuming conservation of volume, vertical (thinning) strain rates equal horizontal dilation rates, and they, 8.9 ± 0.8 nanostrain $a^{-1}$ and 7.4 ± 1.2 nanostrain $a^{-1}$ in northern and southern Tibet, and 12.0 ± 3.2 nanostrain $a^{-1}$ in its southwestern part, suggest no measureable difference. Principal extensional strain rates also are similar in magnitude and orientation. If crustal thinning began at 10–15 Ma and the current rates of horizontal dilation applied both to the entire crust and to that period, the crust should have thinned by 5.5–8.5 km. If isostatic equilibrium applied, the mean elevation of the plateau would have dropped ~1 km. The similar rates for northern, southern, and southwestern Tibet suggest that the processes dictating crustal extension, normal faulting, and crustal thinning in the three regions differ little from one another.

## 1. Introduction

Fault plane solutions of earthquakes, inferences based on satellite imagery, and field studies demonstrate widespread normal faulting, and therefore crustal thinning, of the Tibetan Plateau [e.g., *Armijo et al.,* 1986; *Molnar and Tapponnier*, 1978; *Ni and York*, 1978]. Because normal faulting extracts gravitational potential energy from the lithosphere, and thrust faulting requires work be done against gravity, neither the preponderance of normal faulting (where both elevations and gravitational potential energy are high) nor the occurrence of thrust faulting and crustal thickening on the margins of Tibet should be surprising. Yet perceptions of both the importance and the role of normal faulting in northern Tibet differ. Specifically, *Copley et al.* [2011] considered the normal faulting in northern Tibet to be minor, with strain accumulating largely by strike-slip faulting, whereas others [e.g., *Elliott et al.,* 2010; *England and Houseman*, 1989; *Molnar et al.,* 1993] treated normal faulting in northern and southern Tibet as differing little from one another. We exploit strain rate fields for different parts of Tibet to compare the two views.

East-west extension in southern Tibet is part of an active strain rate field that includes overthrusting of the Himalaya onto India in a direction perpendicular to the local strike of the range; the rigidity of the Indian plate and the curvature of the range require such extension of southern Tibet [e.g., *Armijo et al.,* 1986; *Copley and McKenzie*, 2007; *Jade et al.,* 2004; *Molnar and Chen*, 1982, 1983; *Molnar and Lyon-Caen*, 1989; *Styron et al.,* 2011]. Moreover, because gradients in horizontal normal stresses should, in general, lie parallel to gradients in gravitational potential energy [e.g., *England and Jackson*, 1989; *England and McKenzie*, 1982], the radial overthrusting at the Himalaya is a likely consequence of any rheological structure or vertical distribution of flow, whether that flow occurs without shear on horizontal planes as in a thin viscous sheet [e.g., *England and Molnar*, 1997], as channel flow [e.g., *Clark and Royden*, 2000; *Royden,* 1996], or as a gravity current [*Copley*, 2012; *Copley and McKenzie*, 2007]. Although the mechanical processes responsible for the strain rate field of southern Tibet and the Himalaya, as well as their dependence on gravitational potential energy and surface height, differ, the kinematics of the strain rate fields at the Earth's surface cannot discriminate among hypothesized mechanics without the

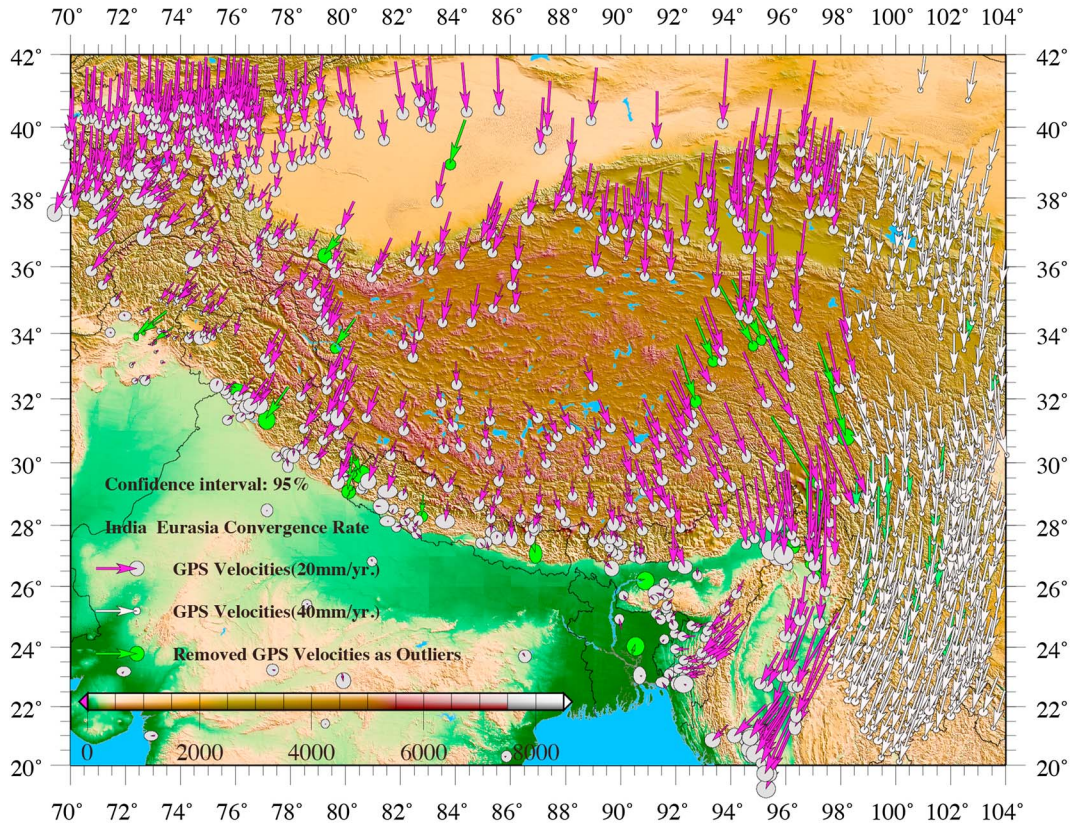


**Figure 1.** Topographic map of Tibetan Plateau and its surrounding, showing GPS velocities relative to the India plate (with 95% confidence ellipses), including some data from other published sources, e.g., Tien Shan [*Zubovich et al.*, 2010], Pamir and Hindu Kush regions [*Ischuk et al.*, 2013; *Mohadjer et al.*, 2010], Himalaya [*Ader et al.*, 2012; *Banerjee and Bürgmann*, 2002; *Banerjee et al.*, 2008; *Bettinelli et al.*, 2006; *Jouanne et al.*, 2014; *Schiffman et al.*, 2013], and Myanmar [*Devachandra et al.*, 2014; *Gahalaut et al.*, 2013; *Maurin et al.*, 2010]. The India-Eurasia rotation pole for an India plate reference frame with respect to Eurasia lies at 27.46° N, 16,12°E with a counterclockwise angular velocity of 0.37 $Ma^{-1}$. These quantities are defined by GPS sites on the India plate with in a region between 70°E and 88°E and 10°N and 25°N. The scale of magenta arrows in west and central Tibet is set twice that of white arrows in eastern Tibet, and green arrows show the GPS velocities that we removed because of large outliers.

exploitation of subtle differences that will be lost in the noise of current velocity fields and likely hidden by elastic strain.

For northern Tibet, citing *Taylor et al.* [2003], *Copley et al.* [2011] inferred that deformation occurs largely by strike-slip faulting "with some minor normal faulting also occurring at fault bends and junctions." *Copley et al.* [2011] then appealed to basal tractions induced by shear on the base of the Tibetan crust by the underthrusting of the Indian plate beneath southern Tibet (as do *Styron et al.* [2015]). Although they do not ignore the great height of Tibet, *Copley et al.* [2011] ignore its large gravitational potential energy. This view contrasts with the alternative that the gravitational potential energy of northern Tibet should, in fact, be greater than that of southern Tibet. Crust beneath northern Tibet is thinner by 10–15 km than that beneath southern Tibet [e.g., *Owens and Zandt*, 1997; *Tseng et al.*, 2009], but elevations are virtually the same. Consequently, the gravitational potential energy per unit area is larger by a few TN/m ($10^{12}$ N/m), a difference comparable to that between lithosphere at mid-ocean ridges and at old oceanic lithosphere [e.g., *Molnar and Stock*, 2009]. Thus, all else equal, we might expect that horizontal extension and crustal thinning to be more rapid in northern than southern Tibet.

Summations of seismic moments do not show different rates of extension in northern and southern Tibet [e.g., *Elliott et al.*, 2010; *Molnar and Chen*, 1983; *Molnar and Lyon-Caen*, 1989], but because the few largest earthquakes dominate such summations, they are not definitive. Although coverage is sparse in some parts of Tibet (Figure 1), GPS velocities, however, can be used to infer strain rates across the region, and we exploit them here to make such a comparison.

## 2. GPS Velocity Field and Its Implications

The horizontal GPS velocity field covering the Tibetan Plateau and its surroundings consists mainly of measurements from the Crustal Movement Observation Network of China (CMONOC). The CMONOC I control points were installed in 1999 and measured in 1999, 2001, 2004, 2007, 2009, and 2011, and the CMONOC II control points were installed in 2009 and measured in 2009 and 2011. Processing of the CMONOC I data yielded the velocity fields of *Zhang et al.* [2004], *Shen et al.* [2005], and *Gan et al.* [2007]. *Li et al.* [2012] updated previous GPS results and produced a velocity solution by processing both the CMONOC I and II data sets using the GAMIT/GLOBK software package [*Herring et al.,* 2010; *McClusky*, 2010].

Besides the CMONOC data, we include velocities from other published sources. The data set of *He et al.* [2013] contains 16 campaign-mode sites located in a localized dense network across central segment of Altyn Tagh Fault from the Tarim Basin to northern Tibet and measured twice in the period of 2009–2011. In addition, we show published velocities for surrounding regions (Figure 1): from the Nepal Himalaya [e.g., *Banerjee et al.,* 2008; *Bettinelli et al.*, 2006; *Bilham et al.,* 1997*; Feldl and Bilham*, 2006], northwest Himalaya [*Banerjee and Bürgmann*, 2002], Pamir-Hindu Kush [*Ischuk et al.,* 2013; *Mohadjer et al.,* 2010], Kashmir and Ladakh Himalaya [e.g., *Jade et al.,* 2004; *Schiffman et al.,* 2013], eastern Himalaya, Naga Hills, and Shillong Plateau [*Devachandra et al.,* 2014; *Vernant et al.,* 2014].

GPS data are scarce in northern Tibet, but observations in that region are essential for this study. To fill the data gap, we include velocities of two control points at the southwest end of a transect of continuous GPS stations. The transect, installed in 2011 [*Ge et al.,* 2014], spans the southern Tarim Basin, the central Altyn Tagh fault, and a region of west-northwest trending fold and thrust faults. We processed the data from these sites together with the regional CMONOC continuous sites for reference using the GAMIT/GLOBK software.

Because some of these sets of velocities are referenced to different reference frames, combining them requires an application of the rigid body rotation to each set, in order to express all site velocities in a common geodetic reference frame, International Terrestrial Reference Frame 2005 (ITRF2005) [*Altamimi et al.,* 2007]. We use the data set of *Li et al.* [2012] as our reference data set and transferred all the other data sets to this reference frame through rigid body rotation about an axis passing through the center of the Earth. This is done by solving for appropriate angular velocities through a least squares procedure, minimizing the velocity postfit residuals of GPS control points common to the data sets of Li et al. and to be rotated. Having transferred all the velocity data sets, we take a mean for those control points that have multiple data entries. We also screened out velocity outliers by visual coherency inspection. We obtain GPS velocities in a Eurasia-fixed reference frame, and through a rigid body rotation, we present velocities in an India-fixed frame (Figure 1, data are provided in the supporting information).

The India-fixed GPS velocity field (Figure 1) shows more clearly how velocities across Tibet vary than if Eurasia defines the reference frame, as is more common. The GPS velocity field shows convergence between Tibetan Plateau and Indian subcontinent, east-west extension of Tibet, and clockwise rotations around the eastern end of the Himalaya.

Most convergence occurs in a narrow belt along the Himalayan arc [e.g., *Banerjee and Bürgmann*, 2002; *Bilham et al.,* 1997; *Feldl and Bilham*, 2006]. In addition, however, approximately north-south convergence also occurs across the Plateau, with velocities relative to India decreasing from southern Tibet to central Tibet [e.g., *Zhang et al.,* 2004], but such that north-south compression is accommodated by east-west extension and is associated with strike-slip faulting on northeast and northwest trending planes [e.g., *Armijo et al.,* 1989; *Elliott et al.,* 2010; *Molnar and Chen*, 1983; *Molnar and Lyon-Caen*, 1989; *Taylor et al.,* 2003]. The rate of east-west extension is enhanced by normal faulting, as discussed above; and consequently, north-south shortening occurs at a lower rate than does the east-west extension.

## 3. Strain Rates Calculation of the Tibetan Plateau

We determined a present-day velocity field using the relatively dense and extensive GPS data and from those velocities a strain rate field (Figure 1). Although only a few GPS sites lie in central Tibet, velocities of them allow us to address strain rates of crustal deformation across the inaccessible, highest-altitude regions, with a large smoothing constant.

We calculated a smooth and continuous strain rate field for the Tibetan Plateau and surroundings from combined GPS data, which is similar to results of *Allmendinger et al.* [2007], *England and Molnar* [2005], and *Gan et al.* [2007], by employing an updated code for interpolation of strain rate [*Shen et al.,* 2015]. At a given site, the horizontal velocity field in its vicinity was approximated by a bilinear function and represented by translation, rotation, and strain rates. The weighted GPS velocities in the neighborhood were used to estimate the parameters through a least squares inversion procedure by minimizing the GPS velocity postfit residuals. For the optimal weightings, we used a distance dependent weighting, $L_i$, assumed to be a Gaussian function, $L_i = exp\left(-\frac{\Delta R^2_i}{D^2}\right)$, multiplied by another function $V_i$ that depends on the area of the Voronoi cell, in which $\Delta R_i$ is the distance between the point in question and a GPS site. The spatial smoothing parameter $D$ is optimally determined with different values for each evaluation site [*Shen et al.,* 2015]. To determine the optimal smoothing distance $D$, we introduce a quantity $Wt$ to denote the threshold of sum of the reweighting coefficients ($W = \Sigma_i\ L_i{*}V_i$) of the data and set $W(D) = Wt$. We present results using $Wt = 24$, 36, and 48, which yield increasing larger estimated values of $D$, because as $Wt$ increases, more GPS data are included, albeit at greater distance from the point than with smaller $Wt$. In Figure 2, we show the interpolated strain rate fields, including principal horizontal shortening, horizontal extensional, and dilatational strain rates, derived from Gaussian/Voronoi cell weighting functions and an example of the smoothing parameter $D$ map, for $Wt = 36$.

To calculate average strain rates in northern, southern, and southwestern Tibet, or the entire Tibet, we use an unweighted analysis of variance ($Wt = 0$) and a large smoothing distance $D$, ~5000 km on the 38, 48, and 22 GPS sites in northern, southern, and southwestern Tibet, respectively, as defined in Figure 3. To estimate uncertainties for average extensional and shortening strain rate and azimuths of principal strain rate, we employ a resampling procedure similar to Bootstrapping methods to determine probability density functions that are approximately Gaussian. For each region, we calculated the strain rate tensor many times, 10,000 for northern Tibet, 16,000 for southern Tibet, and 8000 for southwestern Tibet, by randomly discarding four sites in each calculation for northern and southern Tibet, and three sites for southwestern Tibet to obtain probability density functions (Figure 4). We chose these numbers to be approximately the same fraction of the total number of sites used to estimate average strain rates. Then from the best fitting normal distribution, we estimated means and standard deviations ($1\sigma$).

## 4. Results and Discussion

For the entire Tibetan Plateau, the average maximum extensional strain rate is $20.1 \pm 0.6$ nanostrain $a^{-1}$, oriented N106 ± 1.2°E, and exceeds the orthogonal principal convergence strain rate of $-12.5 \pm 1.0$ nanostrain $a^{-1}$ (Table 1). Thus, dilatational straining occurs at their difference of $7.6 \pm 1.0$ nanostrain $a^{-1}$, which, if volume is conserved, implies vertical contraction, or thinning, at the same rate. As noted above, we focus on the difference between northern and southern Tibet. To define a boundary, we limit southern Tibet to the region where north-south grabens and strike-slip faults connecting them are prominent (Figure 3) [e.g., *Armijo et al.,* 1986, 1989; *Taylor et al.,* 2003].

Three specific areas, bounded by white, pink, and light (pea) green outlines that include normal faulting events recorded in the Global Centroid Moment Tensor catalog 1976–2014 and fault plane solutions of earthquakes within and on the margins of the Tibetan Plateau [*Elliott et al.,* 2010; *Molnar and Lyon-Caen,* 1989], are defined for northern, southern, and southwestern Tibet (Figure 3). We calculated average magnitudes of extensional and shortening strain rates to quantify differences in rates of crustal deformation among the regions. In particular, we also estimate vertical (thinning) strain rates from the average dilatational strain rate.

Average extensional rates (Table 1) occur at comparable rates, though that for southern Tibet is a bit slower than those of northern and southwestern Tibet, and with comparable east-west to ESE-WNW orientations (Figure 4). These orientations are consistent with kinematic analysis of Quaternary terraces and fans in the Shuang Hu graben in northern Tibet, where the orientation of extension is ~120° [*Blisniuk et al.,* 2001], and agree with fault plane solutions [e.g., *Elliott et al.,* 2010; *Molnar and Lyon-Caen,* 1989] and with numerous studies of normal faulting and east-west extension in southern and northeast-southwest extension in southwestern Tibet [e.g., *Edwards and Harrison*, 1997; *Murphy et al.,* 2002; *Garzione et al.,* 2003; *Saylor et al.,* 2010; *Lee et al.,* 2011; *Kali et al.,* 2010; *McCallister et al.,* 2014; *Ryder et al.,* 2012].

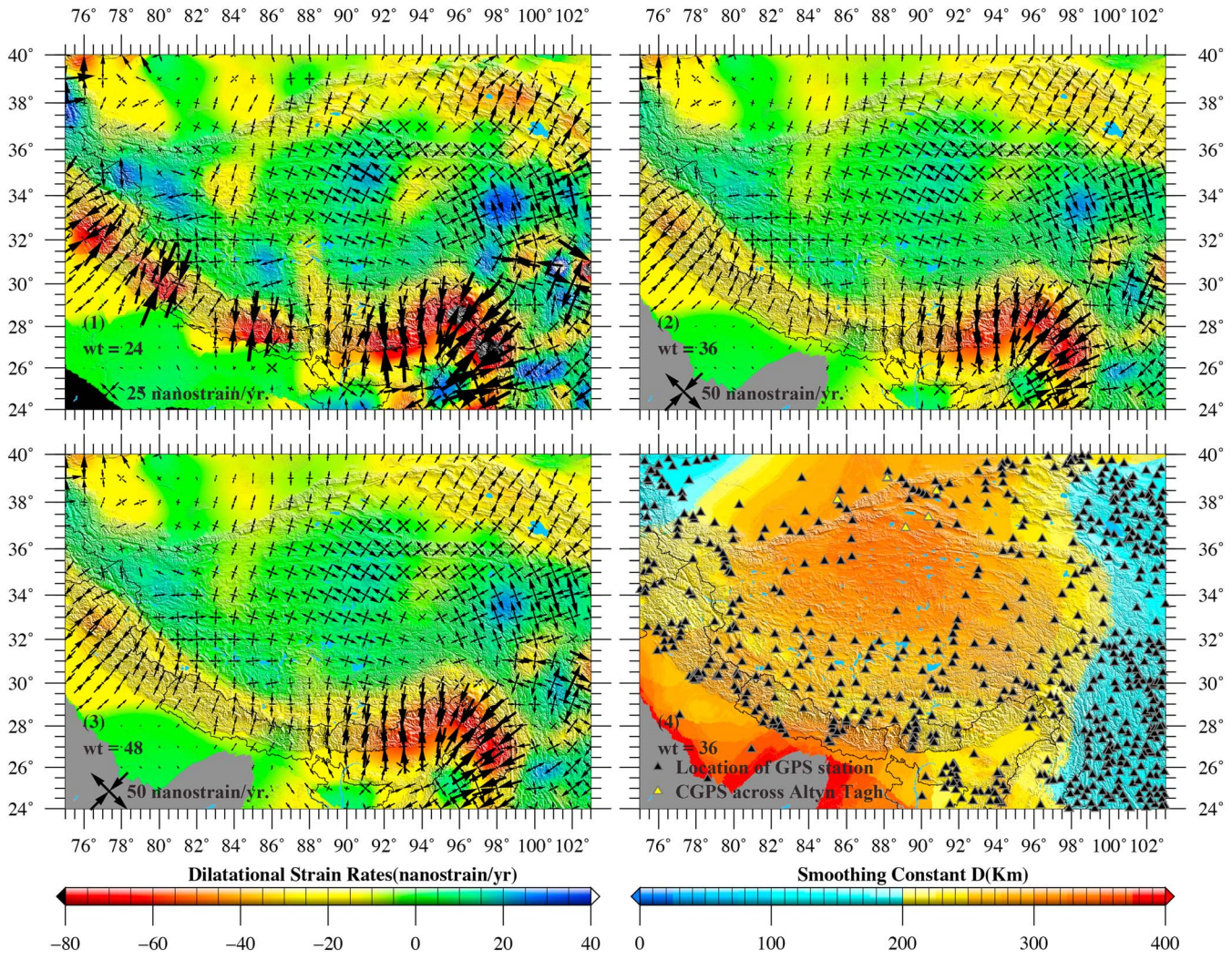


**Figure 2.** Interpolated strain rate results using Gaussian/Voronoi cell weighting functions [*Shen et al.,* 2015] with the net reweighting thresholds set at $Wt = 24$, 36, and 48, respectively, in subplots (1), (2), (3), which show principal strain rates (arrow pairs) on $1° \times 1°$ grids and dilatational strain rate as continuous background color patterns. The largest negative dilatational strain rates lie in the eastern Himalayan syntaxis and in eastern segment of Himalayan Range, −80 to 90 nanostrain $a^{-1}$, and the largest positive dilatational strain rates are close to the epicentral areas of earthquakes in recent decades, approximately 30–50 nanostrain $a^{-1}$. Subplot (4) shows smoothing constant $D$ ($Wt = 36$), and dark triangles denote location of GPS sites used in this study.

Corresponding average principal horizontal shortening strain rates in the three regions again are comparable, with that in the north somewhat more rapid (Table 1). Again assuming conservation of volume, the sum of the three principal strain rates should be zero, and the dilatational rate should equal the vertical strain rate. The larger shortening rate in northern than southern or southwestern Tibet therefore suggests that the strike-slip component of strain is 35–40% greater in northern than southern Tibet, as *Copley et al.* [2011] inferred.

The average extensional and dilatational strain rates in southwestern Tibet are larger than those in northern and southern Tibet, but with larger uncertainties for each component, differences are not significant. More important, however, average rates of dilatational strain, $8.9 \pm 0.8$ nanostrain $a^{-1}$ in northern Tibet, $7.4 \pm 1.2$ nanostrain $a^{-1}$ in southern Tibet, and $12.0 \pm 3.2$ nanostrain $a^{-1}$ (Table 1 and Figure 4), differ little from one another, or from the average for the entire plateau, $-7.6 \pm 1.0$ nanostrain $a^{-1}$. These essentially similar thinning rates for the three regions are not consistent with the extension in northern Tibet being the result of accommodation of strike slip at the ends of such faults but are consistent with an outward spreading of the plateau in response to greater potential energy per unit area than in the surroundings.

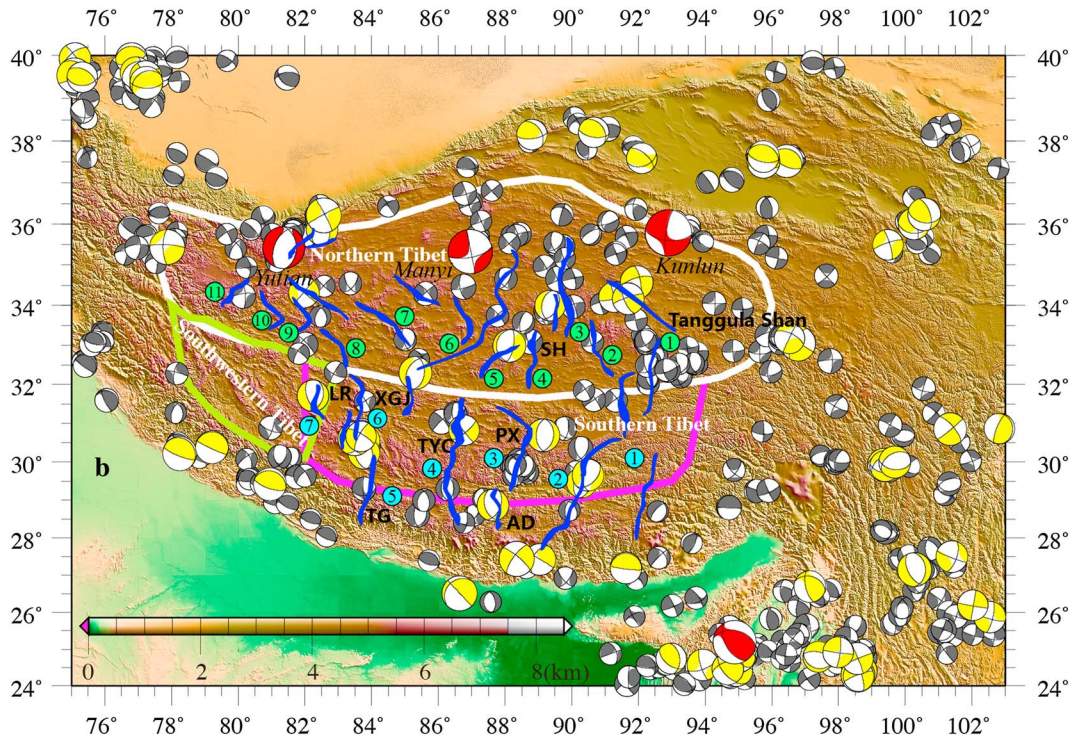


**Figure 3.** Earthquake focal mechanisms from the Global CMT (Centroid Moment Tensor) catalogue from 1 January 1976 to 1 December 2014 and outlines of northern, southern, and southwestern Tibet. Red beach balls indicate earthquakes with $7.9 \geq M_w \geq 7.0$: the 2008 Yutian earthquake in western Tibet, the 1997 Manyi and 2001 Kunlun earthquakes in central and northern Tibet, and the 1988 $M_w$7.2 Myanmar earthquake. Yellow beach balls are for earthquakes with $6.9 \geq M_w \geq 6$, and gray beach balls for $5.9 \geq M_w \geq 5$. Blue belts in Tibet show ~7 rifts and grabens in southern Tibet and ~11 rifts and grabens in central and northern Tibet, marked with a number for each rift or graben.

Although fault plane solutions of earthquakes show little difference in normal faulting between northern and southern Tibet, geologic evidence for normal faulting is much stronger in southern than northern Tibet, surely in part because the southern part is the more accessible and also because topographic relief associated with northerly trending grabens in southern Tibet is greater than that in most of northern Tibet [e.g., *Armijo et al.,* 1986]. Dating of grabens throughout Tibet, but mostly in southern Tibet, has yielded onsets of such normal faulting since 15 Ma, and in some cases closer to 10 Ma. For southernmost Tibet near the Himalaya, dates for different grabens from west to east are 9 Ma [*Murphy et al.,* 2002; *Saylor et al.,* 2010], 14–13 Ma [*McCallister et al.,* 2014], ~11 Ma [*Garzione et al.,* 2003], ~13–12 Ma [*Lee et al.,* 2011], 13–12 Ma [*Kali et al.,* 2010], and <12.5 Ma [*Edwards and Harrison*, 1997]. Farther north but still in southern Tibet, similar ages include 11–8 Ma [*Woodruff et al.,* 2013], 16–12 Ma [*Styron et al.,* 2013], and ~8 Ma [*Harrison et al.,* 1995; *Pan and Kidd*, 1992]. To the best of our knowledge, only one graben from northern Tibet has been dated, at ~13.5 Ma by *Blisniuk et al.* [2001].

Obviously, with an onset date for only one graben in the north, the timing of normal faulting there is constrained less well than in the south. Nevertheless, suppose that most of the normal faulting and crustal thinning have occurred since 15 (or 10) Ma. Then, with rates of thinning of ~8 nanostrain $a^{-1}$ since 15 (or 10) Ma, total vertical strains would be 0.12 (or 0.8); and if such strains reflected thinning of the entire crust 70 km thick, the thinning would be 8.4 (or 5.6) km. If Airy isostasy applied, the surface would have dropped ~1 km. Obviously, if only the upper crust underwent thinning, the elevation drop would be smaller than 1 km. The occurrence of earthquakes within the mantle beneath southern Tibet and showing normal faulting, however, suggests that the mantle there undergoes straining similar to that in the overlying crust [e.g., *Chen et al.,* 1981; *de la Torre et al.,* 2007; *Molnar and Chen*, 1983]. Moreover, radial anisotropy beneath most of the Tibetan Plateau is consistent with crustal thinning through most of the crust [*Shapiro et al.,* 2004; *Xie et al.,* 2013]. A more recent onset of thinning in the north than south would lead to less thinning in the north and might account for the less well developed grabens in the north than south.

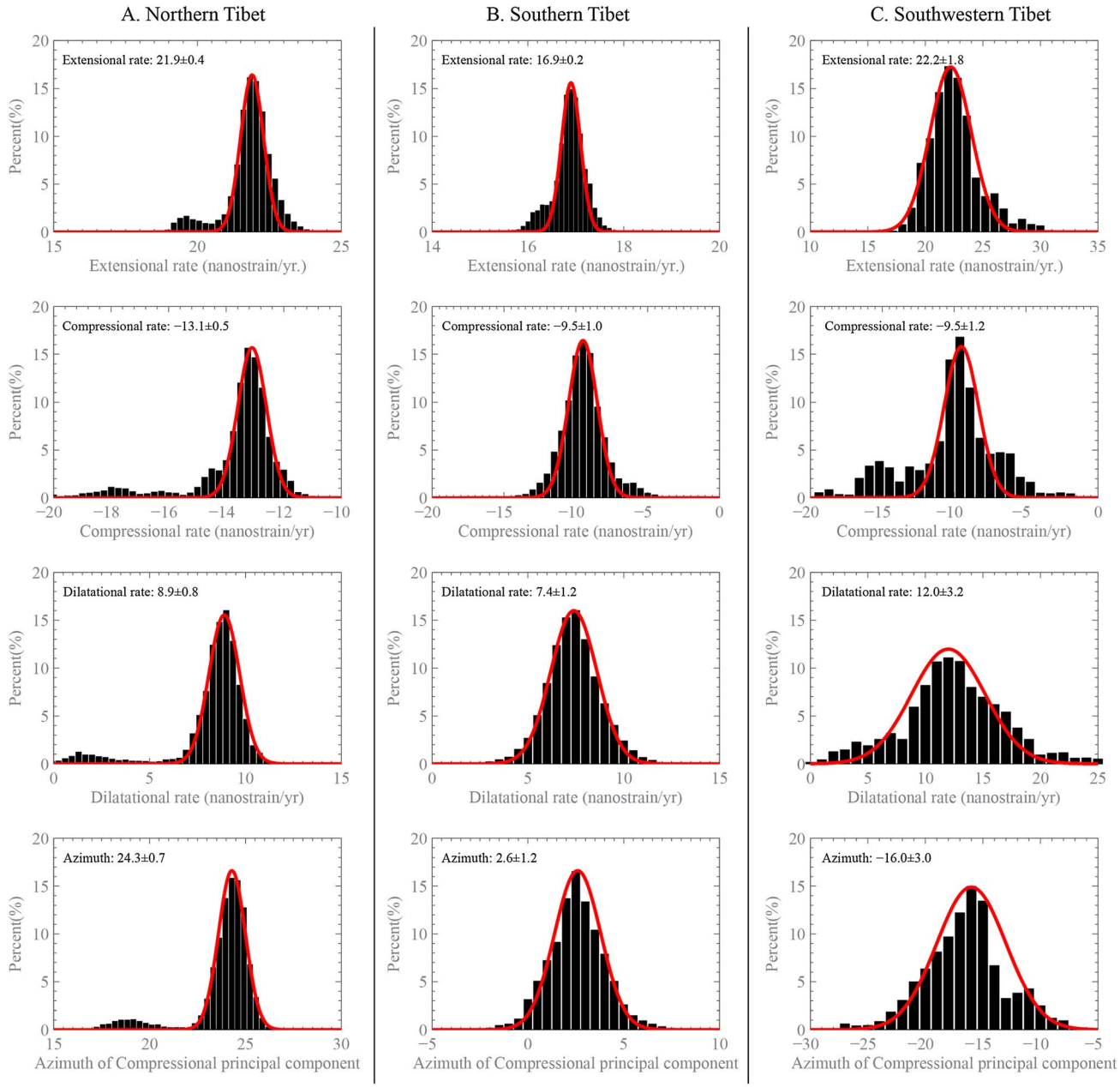


**Figure 4.** Uncertainty calculations of strain rates in northern, southern, and southwestern Tibet, with normal distribution fits using a Bootstrapping resampling statistical method. The error range is 1$\sigma$, ~67% confidence interval.

**Table 1.** Principle Components of Strain Rates for Tibet

| Region | Horizontal Extension Rate (nanostrain $a^{-1}$) | Horizontal Extension Orientation | Horizontal Shortening Rate (nanostrain $a^{-1}$) | Vertical Shortening Rate (nanostrain $a^{-1}$) |
|---|---|---|---|---|
| All | 20.1 ± 0.6 | N106 ± 1.2°E | −12.5 ± 1.0 | −7.6 ± 1.0 |
| Northern | 21.9 ± 0.4 | N114 ± 0.7°E | −13.1 ± 0.5 | −8.9 ± 0.8 |
| Southern | 16.9 ± 0.2 | N93 ± 1.2°E | −9.5 ± 1.0 | −7.4 ± 1.2 |
| Southwestern | 22.2 ± 1.8 | N74 ± 3.0°E | −9.5 ± 1.2 | −12.0 ± 3.2 |

In summary, the present-day strain rates suggest that northern and southern Tibet behave similarly, and therefore presumably respond to the same overall geodynamic processes. An extrapolation of these strain rates for the period since normal faulting associated with east-west extension began suggests that the surface elevation of the plateau should have dropped ~1000 m since 10–15 Ma.

**Acknowledgments**
We thank all of our Chinese colleagues who constructed the network and collected the GPS measurements. W.-P. G. thanks Min Wang for guidance in GPS analysis. P.C. England and G.A. Houseman offered prompt, constructive reviews of the manuscript. This work was jointly supported by the Natural Science Foundation of China (grants 41304035 and 41090294), the Basic Research Project of Institute of Earthquake Science, China Earthquake Administration (grant 2014IESLZ05), and the U.S. National Science Foundation under grants EAR 1211378 and 1246925, and a scholarship from China Scholarship Council (CSC) under the grant CSC 201304190034. Some figures used the GMT software [*Wessel and Smith*, 1998].

The Editor thanks Philip England and an anonymous reviewer for their assistance in evaluating this paper.

## References

Ader, T., et al. (2012), Convergence rate across the Nepal Himalaya and interseismic coupling on the Main Himalayan Thrust: Implications for seismic hazard, *J. Geophys. Res.*, *117*, B04403, doi:10.1029/2011JB009071.

Allmendinger, R. W., R. Reilinger, and J. Loveless (2007), Strain and rotation rate from GPS in Tibet, Anatolia, and the Altiplano, *Tectonics*, *26*, TC3013, doi:10.1029/2006TC002030.

Altamimi, Z., X. Collilieux, J. Legrand, B. Garayt, and C. Boucher (2007), ITRF2005: A new release of the International Terrestrial Reference Frame based on time series of station positions and Earth Orientation Parameters, *J. Geophys. Res.*, *112*, B09401, doi:10.1029/2007JB004949.

Armijo, R., P. Tapponnier, J.-L. Mercier, and T.-L. Han (1986), Quaternary extension in southern Tibet: Field observations and tectonic implications, *J. Geophys. Res.*, *91*, 13,803–13,872, doi:10.1029/JB091iB14p13803.

Armijo, R., P. Tapponnier, and T. Han (1989), Late Cenozoic right-lateral strike-slip faulting in southern Tibet, *J. Geophys. Res.*, *94*, 2787–2838, doi:10.1029/JB094iB03p02787.

Banerjee, P., and R. Bürgmann (2002), Convergence across the northwest Himalaya from GPS measurements, *Geophys. Res. Lett.*, *29*(13), 1652, doi:10.1029/2002GL015184.

Banerjee, P., R. Bürgmann, B. Nagarajan, and E. Apel (2008), Intraplate deformation of the Indian subcontinent, *Geophys. Res. Lett.*, *35*, L18301, doi:10.1029/2008GL035468.

Bettinelli, P., J.-P. Avouac, M. Flouzat, F. Jouanne, L. Bollinger, P. Willis, and G. R. Chitrakar (2006), Plate motion of India and interseismic strain in the Nepal Himalayan from GPS and DORIS measurements, *J. Geod.*, *80*, 567–589.

Bilham, R., K. Larson, J. Freymueller, and Project Idylhim Members (1997), GPS measurements of present-day convergence across the Nepal Himalaya, *Nature*, *386*, 61–64.

Blisniuk, P. M., B. R. Hacker, J. Glodny, L. Ratschbacher, S. W. Bi, Z. H. Wu, M. O. McWilliams, and A. Calvert (2001), Normal faulting in central Tibet since at least 13.5 Myr ago, *Nature*, *412*(6847), 628–632.

Chen, W.-P., J. L. Nábělek, T. J. Fitch, and P. Molnar (1981), An intermediate depth earthquake beneath Tibet: Source characteristics of the event of September 14, 1976, *J. Geophys. Res.*, *86*, 2863–2876, doi:10.1029/JB086iB04p02863.

Clark, M. K., and L. H. Royden (2000), Topographic ooze: Building the eastern margin of Tibet by lower crustal flow, *Geology*, *28*, 703–706.

Copley, A. (2012), The formation of mountain range curvature by gravitational spreading, *Earth Planet. Sci. Lett.*, *351–352*, 208–214.

Copley, A., and D. McKenzie (2007), Models of crustal flow in the India-Asia collision zone, *Geophys. J. Int.*, *169*(2), 683–698.

Copley, A., J. P. Avouac, and B. P. Wernicke (2011), Evidence for mechanical coupling and strong Indian lower crust beneath southern Tibet, *Nature*, *472*(7341), 79–81.

de la Torre, T. L., G. Monsalve, A. F. Sheehan, S. Sapkota, and F. Wu (2007), Earthquake processes of the Himalayan collision zone in eastern Nepal and the southern Tibetan Plateau, *Geophys. J. Int.*, *171*, 718–738.

Devachandra, M., B. Kundu, J. Catherine, A. Kumar, and V. K. Gahalaut (2014), Global Positioning System (GPS) measurements of crustal deformation across the frontal eastern Himalayan syntaxis and seismic-hazard assessment, *Bull. Seismol. Soc. Am.*, *104*(3), 1518–1524.

Edwards, M. A., and T. M. Harrison (1997), When did the roof collapse? Late Miocene north–south extension in the high Himalaya revealed by Th-Pb monazite dating of the Khula Kangri granite, *Geology*, *25*, 543–546.

Elliott, J. R., R. J. Walters, P. C. England, J. A. Jackson, Z. Li, and B. Parsons (2010), Extension on the Tibetan Plateau: Recent normal faulting measured by InSAR and body wave seismology, *Geophys. J. Int.*, *183*, 503–535.

England, P., and J. Jackson (1989), Active deformation of the continents, *Annu. Rev. Earth Planet. Sci.*, *17*, 197–226.

England, P., and D. McKenzie (1982), A thin viscous sheet model for continental deformation, *Geophys. J. Int.*, *70*(2), 295–321.

England, P., and P. Molnar (1997), Active deformation of Asia: From kinematics to dynamics, *Science*, *278*, 647–650.

England, P., and P. Molnar (2005), Late Quaternary to decadal velocity fields in Asia, *J. Geophys. Res.*, *110*, B12401, doi:10.1029/2004JB003541.

England, P. C., and G. A. Houseman (1989), Extension during continental convergence, with application to the Tibetan Plateau, *J. Geophys. Res.*, *94*, 17,561–17,579, doi:10.1029/JB094iB12p17561.

Feldl, N., and R. Bilham (2006), Great Himalayan earthquakes and the Tibetan Plateau, *Nature*, *444*, 165–170.

Gahalaut, V. K., et al. (2013), Aseismic plate boundary in the Indo-Burmese wedge, northwest Sunda Arc, *Geology*, *41*, 235–238.

Gan, W. J., P. Z. Zhang, Z. K. Shen, Z. J. Niu, M. Wang, Y. G. Wan, D. M. Zhou, and J. Cheng (2007), Present-day crustal motion within the Tibetan Plateau inferred from GPS measurements, *J. Geophys. Res.*, *112*, B08416, doi:10.1029/2005JB004120.

Garzione, C. N., P. G. DeCelles, D. G. Hodkinson, T. P. Ojha, and B. N. Upreti (2003), East–west extension and Miocene environmental change in the southern Tibetan Plateau: Thakkhola graben, central Nepal, *Geol. Soc. Am. Bull.*, *115*, 3–20.

Ge, W. P., Z. K. Shen, D. Y. Yuan, M. Wang, Y. S. Shao, P. C. He, and B. Zhang (2014), Contemporary localized orogenic process along the central segment of Altyn Tagh Fault using continuous GPS observation in Northern Tibetan Plateau, Abstract and Poster G11B-0492 presented at 2014 Fall Meeting, AGU, San Francisco, Calif., 15 Dec.

Harrison, T. M., P. Copeland, W. S. F. Kidd, and O. M. Lovera (1995), Activation of the Nyainqentanghla shear zone: Implications for uplift of the southern Tibetan Plateau, *Tectonics*, *14*, 658–676, doi:10.1029/95TC00608.

He, J., P. Vernant, J. Chéry, W. Wang, S. Lu, W. Ku, W. Xia, and R. Bilham (2013), Nailing down the slip rate of the Altyn Tagh fault, *Geophys. Res. Lett.*, *40*, 5382–5386, doi:10.1002/2013GL057497.

Herring, T. A., R. W. King, and S. C. McClusky (2010), GAMIT: GPS analysis at MIT-Release 10.4, pp. 1–171, MIT. [Available at http://www-gpsg.mit.edu/~simon/gtgk/GAMIT_Ref.pdf.]

Ischuk, A., et al. (2013), Kinematics of the Pamir and Hindu Kush regions from GPS geodesy, *J. Geophys. Res. Solid Earth*, *118*, 2408–2416, doi:10.1002/jgrb.50185.

Jade, S., B. C. Bhatt, R. Bendick, V. K. Gaur, P. Molnar, M. B. Anand, and D. Kumar (2004), GPS measurements from the Ladakh Himalaya, India: Preliminary tests of plate-like or continuous deformation in Tibet, *Geol. Soc. Am. Bull.*, *116*, 1385–1391.

Jouanne, F., A. Awan, A. Pêcher, A. Kausar, J. L. Mugnier, I. Khan, N. A. Khan, and J. Van Melle (2014), Present-day deformation of northern Pakistan from Salt Ranges to Karakorum Ranges, *J. Geophys. Res. Solid Earth*, *119*, 2487–2503, doi:10.1002/2013JB010776.

Kali, E., P. H. Leloup, N. Arnaud, G. Mahéo, D. Liu, E. Boutonnet, J. Van der Woerd, X. Liu, J. Liu-Zeng, and H. Li (2010), Exhumation history of the deepest central Himalayan rocks, Ama Drime range: Key pressure-temperature-deformation-time constraints on orogenic models, *Tectonics*, *29*, TC2014, doi:10.1029/2009TC002551.

Lee, J., C. Hager, S. R. Wallis, D. F. Stockli, M. J. Whitehouse, M. Aoya, and Y. Wang (2011), Middle to late Miocene extremely rapid exhumation and thermal reequilibration in the Kung Co rift, southern Tibet, *Tectonics*, *30*, TC2007, doi:10.1029/2010TC002745.

Li, Q., X. You, S. Yang, R. Du, X. Qiao, R. Zou, and Q. Wang (2012), A precise velocity field of tectonic deformation in China as inferred from intensive GPS observations, *Sci. China Earth Sci.*, *55*(5), 695–698.

Maurin, T., F. Masson, C. Rangin, U. T. Min, and P. Collard (2010), First global positioning system results in northern Myanmar: Constant and localized slip rate along the Sagaing fault, *Geology*, *38*(7), 591–594.

McCallister, A. T., M. H. Taylor, M. A. Murphy, R. H. Styron, and D. F. Stockli (2014), Thermochronologic constraints on the Late Cenozoic exhumation history of the Gurla Mandhata metamorphic core complex, southwestern Tibet, *Tectonics*, *33*, 27–52, doi:10.1002/2013TC003302.

McClusky, S. C. (2010), GLOBK: Global Kalman filter VLBI and GPS analysis program—Version 10.4, pp. 1–95, MIT. [Available at http://www-gpsg.mit.edu/~simon/gtgk/GLOBK_Ref.pdf.]

Mohadjer, S., et al. (2010), Partitioning of India-Eurasia convergence in the Pamir-Hindu Kush from GPS measurements, *Geophys. Res. Lett.*, *37*, L04305, doi:10.1029/2009GL041737.

Molnar, P., and W. P. Chen (1982), Seismicity and mountain building, in *Mountain Building Processes*, edited by K. Hsü, pp. 41–57, Academic Press, London.

Molnar, P., and W. P. Chen (1983), Focal depths and fault plane solutions of earthquakes under the Tibetan Plateau, *J. Geophys. Res.*, *88*, 1180–1196, doi:10.1029/JB088iB02p01180.

Molnar, P., and H. Lyon-Caen (1989), Fault plane solutions of earthquakes and active tectonics of the Tibetan Plateau and its margins, *Geophys. J. Int.*, *99*, 123–153.

Molnar, P., and J. M. Stock (2009), Slowing of India's convergence with Eurasia since 20 Ma and its implications for Tibetan mantle dynamics, *Tectonics*, *28*, TC3001, doi:10.1029/2008TC002271.

Molnar, P., and P. Tapponnier (1978), Active tectonics of Tibet, *J. Geophys. Res.*, *83*, 5361–5375, doi:10.1029/JB083iB11p05361.

Molnar, P., P. England, and J. Martinod (1993), Mantle dynamics, uplift of the Tibetan Plateau, and the Indian monsoon, *Rev. Geophys.*, *31*, 357–396, doi:10.1029/93RG02030.

Murphy, M. A., A. Yin, P. Kapp, T. M. Harrison, C. E. Manning, F. J. Ryerson, L. Ding, and J. Guo (2002), Structural evolution of the Gurla Mandhata detachment system, southwest Tibet: Implications for the eastward extent of the Karakoram fault system, *Geol. Soc. Am. Bull.*, *114*, 428–447.

Ni, J., and J. E. York (1978), Late Cenozoic extensional tectonics of the Tibetan Plateau, *J. Geophys. Res.*, *83*, 5377–5384, doi:10.1029/JB083iB11p05377.

Owens, T. J., and G. Zandt (1997), Implications of crustal property variations for models of Tibetan Plateau evolution, *Nature*, *387*(6628), 37–43.

Pan, Y., and W. S. F. Kidd (1992), Nyainqentanglha shear zone: A late Miocene extensional detachment in the southern Tibetan Plateau, *Geology*, *20*, 775–778.

Royden, L. H. (1996), Coupling and decoupling of crust and mantle in convergent orogens: Implications for strain partitioning in the crust, *J. Geophys. Res.*, *101*, 17,679–17,705, doi:10.1029/96JB00951.

Ryder, I., R. Bürgmann, and E. Fielding (2012), Static stress interactions in extensional earthquake sequences: An example from the South Lunggar Rift, Tibet, *J. Geophys. Res.*, *117*, B09405, doi:10.1029/2012JB009365.

Saylor, J., P. DeCelles, G. Gehrels, M. Murphy, R. Zhang, and P. Kapp (2010), Basin formation in the High Himalaya by arc-parallel extension and tectonic damming: Zhada Basin, southwestern Tibet, *Tectonics*, *29*, TC1004, doi:10.1029/2008TC002390.

Schiffman, C., B. S. Bali, W. Szeliga, and R. Bilham (2013), Seismic slip deficit in the Kashmir Himalaya from GPS observations, *Geophys. Res. Lett.*, *40*, 5642–5645, doi:10.1002/2013GL057700.

Shapiro, N. M., M. H. Ritzwoller, P. Molnar, and V. Levin (2004), Thinning and flow of Tibetan crust constrained by the seismic anisotropy, *Science*, *305*, 233–236.

Shen, Z.-K., J. Lü, M. Wang, and R. Bürgmann (2005), Contemporary crustal deformation around the southeast borderland of the Tibetan Plateau, *J. Geophys. Res.*, *110*, B11409, doi:10.1029/2004JB003421.

Shen, Z.-K., M. Wang, Y. Zeng, and F. Wang (2015), Optimal interpolation of spatially discretized geodetic data, *Bull. Seismol. Soc. Am.*, in press.

Styron, R. H., M. H. Taylor, and M. A. Murphy (2011), Oblique convergence, arc-parallel extension, and the role of strike-slip faulting in the High Himalaya, *Geosphere*, *7*, 582–596.

Styron, R. H., M. H. Taylor, K. E. Sundell, D. F. Stockli, J. A. G. Oalmann, A. Möller, A. T. McCallister, D.-l. Liu, and L. Ding (2013), Miocene initiation and acceleration of extension in the South Lunggar rift, western Tibet: Evolution of an active detachment system from structural mapping and (U-Th)/He thermochronology, *Tectonics*, *32*, 880–907, doi:10.1002/tect.20053.

Styron, R. H., M. Taylor, and K. Sundell (2015), Accelerated extension of Tibet linked to the northward underthrusting of Indian crust, *Nat. Geosci.*, *8*, 131–134.

Taylor, M., A. Yin, F. J. Ryerson, P. Kapp, and L. Ding (2003), Conjugate strike-slip faulting along the Bangong-Nujiang suture zone accommodates coeval east–west extension and north–south shortening in the interior of the Tibetan Plateau, *Tectonics, 22*(4), 1044, doi:10.1029/2002TC001361.

Tseng, T.-L., W.-P. Chen, and R. L. Nowack (2009), Northward thinning of Tibetan crust revealed by virtual seismic profiles, *Geophys. Res. Lett.*, *36*, L24304, doi:10.1029/2009GL040457.

Vernant, P., R. Bilham, W. Szeliga, D. Drupka, S. Kalita, A. K. Bhattacharyya, V. K. Gaur, P. Pelgay, R. Cattin, and T. Berthet (2014), Clockwise rotation of the Brahmaputra Valley relative to India: Tectonic convergence in the eastern Himalaya, Naga Hills, and Shillong Plateau, *J. Geophys. Res. Solid Earth*, *119*, 6558–6571, doi:10.1002/2014JB011196.

Wessel, P., and W. H. F. Smith (1998), New, improved version of Generic Mapping Tools released, *Eos Trans. AGU*, *79*(47), 579, doi:10.1029/98EO00426.

Woodruff, W. H., Jr., B. K. Horton, P. Kapp, and D. F. Stockli (2013), Late Cenozoic evolution of the Lunggar extensional basin, Tibet: Implications for basin growth and exhumation in hinterland plateaus, *Geol. Soc. Am. Bull.*, *125*, 343–358.

Xie, J., M. H. Ritzwoller, W. Shen, Y. Yang, Y. Zheng, and L. Zhou (2013), Crustal radial anisotropy across Eastern Tibet and the Western Yangtze Craton, *J. Geophys. Res. Solid Earth*, *118*, 4226–4252, doi:10.1002/jgrb.50296.

Zhang, P.-Z., et al. (2004), Continuous deformation of the Tibetan Plateau from global positioning system data, *Geology*, *32*(9), 809–812.

Zubovich, A. V., et al. (2010), GPS velocity field for the Tien Shan and surrounding regions, *Tectonics*, *29*, TC6014, doi:10.1029/2010TC002772.